Sodium-Ion Batteries

Deutsche Ausgabe: DOI: 10.1002/ange.201606415
Internationale Ausgabe: DOI: 10.1002/anie.201606415

Sodium and Manganese Stoichiometry of P2-Type $Na_{2/3}MnO_2$

*Shinichi Kumakura, Yoshiyuki Tahara, Kei Kubota, Kuniko Chihara, and Shinichi Komaba**

Abstract: *To realize a reversible solid-state $Mn^{III/IV}$ redox couple in layered oxides, co-operative Jahn–Teller distortion (CJTD) of six-coordinate Mn^{III} (t_{2g}^3–e_g^1) is a key factor in terms of structural and physical properties. We develop a single-phase synthesis route for two polymorphs, namely distorted and undistorted P2-type $Na_{2/3}MnO_2$ having different Mn stoichiometry, and investigate how the structural and stoichiometric difference influences electrochemical reaction. The distorted $Na_{2/3}MnO_2$ delivers 216 mAh g^{-1} as a 3 V class positive electrode, reaching 590 Wh (kg oxide)$^{-1}$ with excellent cycle stability in a non-aqueous Na cell and demonstrates better electrochemical behavior compared to undistorted $Na_{2/3}MnO_2$. Furthermore, reversible phase transitions correlated with CJTD are found upon (de)sodiation for distorted $Na_{2/3}MnO_2$, providing a new insight into utilization of the $Mn^{III/IV}$ redox couple for positive electrodes of Na-ion batteries.*

Recently, Na-ion batteries have been intensively studied for future application, including grid-scale storages, owing to favorable sodium availability.[1] Among various positive electrode materials, layered sodium transition metal oxides (Na_xMO_2) based on abundant metals have attracted continuous attention,[2] and especially Mn-based materials meet requirements for low cost battery systems without sacrificing energy density and safety.[3] Besides their industrial benefit, Na_xMnO_2 stimulates scientific interests owing to its unique phase variation. Phase diversity of Na_xMnO_2 usually depends on the Na/Mn ratio,[4] and each phase has been discussed based on the criteria reported in 1980.[5] In accordance with this manner, layered Na_xMnO_2 has several polymorphs, so-called P2- and O3-type, classified by different MnO_2-slab stacking along *c*-axis. Their electrochemical Na extraction/insertion was firstly reported by Mendiboure et al. in 1985.[6] A valence state of Mn also affects the polymorphism, and in particular, six-coordinate Mn^{III} (t_{2g}^3–e_g^1) leads to distorted phase variation owing to co-operative Jahn–Teller distortion (CJTD). In electrochemical discussions, since the $Mn^{III/IV}$ redox couple is thought to cause large and anisotropic volume change[2,7] and localization of cations and electrons owing to a long-range ordering of Na^+/vacancies and the honeycomb structure of $Mn^{III/IV}$,[8] Mn^{III} ions have been regarded as unfavorable components that should be ruled out from targeted materials for battery application. Therefore, a recent strategy has been based on the idea to keep average oxidation state of manganese close to +4 to avoid the Jahn–Teller effect of Mn^{III} by substitution with other mono- or divalent cations.[7b,9] However, we find no reports to fully understand and solve drawback of CJTD in layered Na_xMnO_2. In this study, we focus on P2-type $Na_{2/3}MnO_2$ polymorphs as basic Mn redox materials with/without CJTD. By preparing high-purity samples of the P2-$Na_{2/3}MnO_2$ polytypes and discussing how the polymorphic characteristics bring difference in electrochemical and structural properties during (de)sodiation, we demonstrate high reversibility of the $Mn^{III/IV}$ redox couple involving CJTD in layered oxides.

The distorted polymorph with an orthorhombic lattice is denoted by adding an additional prime symbol (P′2-Na_xMnO_2).[4,10] Crystallization of P2- and P′2-Na_xMnO_2 is highly dependent on synthesis conditions, such as the heating process and Na/Mn ratio.[4,7b] P′2-Na_xMnO_2 is obtained by quenching from over 1000 °C, while synthesis of P2-Na_xMnO_2 requires a slow cooling process after heating to circa 1000 °C.[7b,10] Because of uncontrollable Na loss during firing, P2/P′2 mixed phase[10b] and/or monoclinic impurity phases[7b,10a] always came out together in previous studies. During the cooling process, Mn^{III} in P′2-Na_xMnO_2 tends to be Mn^{IV} having no distortion, and simultaneously oxygen uptake occurs for charge compensation, which results in creating vacancy in Mn layer.[4,10b,11] Parant et al. first reported the crystal structure, Jahn–Teller effect on the lattice, sensitivity of the synthesis, and implication of Mn vacancy for the polymorphs in 1971.[4] Based on these knowledge, we stood for the idea that single phase of P2-Na_xMnO_2 can be only obtained from pure P′2-Na_xMnO_2 without Na loss, and we first optimized synthesis condition for pure P′2-$Na_{2/3}MnO_2$. Detailed synthesis conditions and X-ray diffraction (XRD) patterns are given in the Supporting Information, Figure S1, and hereafter we term P2- and P′2-$Na_{2/3}MnO_2$ samples as *h*-NMO and *o*-NMO, respectively. Our optimization of the synthesis for *o*-NMO shows that only a 50 °C difference led to impurities, which could be detected only by synchrotron XRD (SXRD) measurements. As shown in Figure 1 a, heating up to 1050 °C followed by quench is the best synthesis condition to obtain pure *o*-NMO, and all the diffraction peaks, except a peak at $2\theta = 7.8°$ indicated as ▼, can be indexed as P′2-type layered structure (S.G.*Cmcm*), whereas *h*-NMO was obtained by heating up *o*-NMO again to 700 °C followed by slow cooling to 500 °C and quench. Figure 1 b shows an SXRD pattern of *h*-NMO, and all of the diffraction peaks can be indexed as a P2-type structure (space group $P6_3/mmc$). As we

[*] S. Kumakura, Y. Tahara, Dr. K. Kubota, K. Chihara, Prof. S. Komaba
Department of Applied Chemistry, Tokyo University of Science
Shinjuku, Tokyo 162–8601 (Japan)
E-mail: komaba@rs.kagu.tus.ac.jp
S. Kumakura
Umicore Japan KK
1-2-3 Kita-Aoyama, Minato-ku Tokyo, 107-0061 (Japan)
Dr. K. Kubota, Prof. S. Komaba
Elements Strategy Initiative for Catalysts & Batteries (ESICB)
Kyoto University
1–30 Goryo-Ohara, Nishikyo-ku, Kyoto 615-8245 (Japan)

Supporting information for this article can be found under: http://dx.doi.org/10.1002/anie.201606415.

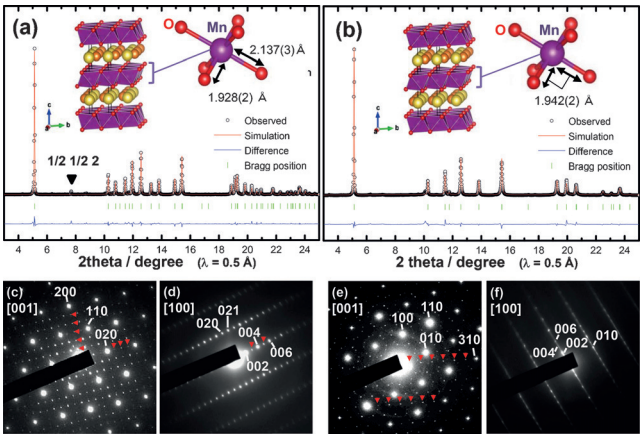

Figure 1. SXRD patterns and fitting result by the Rietveld analysis on a) *o*-NMO and b) *h*-NMO. Electron diffraction patterns of *o*-NMO along c) [001] and d) [100] and of *h*-NMO along e) [001] and f) [100]. The superstructure reflections are indicated by red arrows. TEM images of the corresponding area to that of the diffraction measurement are shown in the Supporting Information, Figure S3.

expected, *h*-NMO was successfully obtained without impurity, and this is the first report to characterize structure of the pure P2-$Na_{2/3}MnO_2$ based on SXRD. Then, we conducted Rietveld analysis by using RIETAN-FP.[12] *R* factors for both samples become adequately low, and the lattice constant of *o*-NMO well agrees with previous reports (Supporting Information, Table S1).[7b,10b] The ratio of lattice constant of *o*-NMO is calculated to be $b_{ortho}/a_{ortho} = 1.87$, suggesting huge distortion owing to longer *b* and shorter *a* axes compared to $b_{ortho}/a_{hexa} = \sqrt{3}$ for the hexagonal lattice, and the degree of distortion, δ, is estimated to 8 % (the in-plane arrangement of *o*-/*h*-NMO and the definition of δ are given in the Supporting Information, Figure S2). The anisotropic Mn–O bond length obtained by the refinement is also shown in the inset of Figure 1. Table 1

Table 1: The summary of compositional analyses.

Sample	Mn oxidation state	Na/Mn ratio	O/Mn ratio	Composition
o-NMO	+3.37	0.64	2.00	$Na_{0.64}Mn^{+3}_{0.63}Mn^{+4}_{0.37}O_2$
h-NMO	+3.76	0.65	2.21	$Na_{0.59}Mn^{+3}_{0.16}Mn^{+4}_{0.74}\square_{0.10}O_2$

shows that *o*-/*h*-NMO have an identical Na/Mn ratio from ICP analysis. By combining results of iodometry for the average oxidation state of Mn, the chemical formula of *o*- and *h*-NMO were determined as $Na_{0.64}MnO_2$ and $Na_{0.59}Mn_{0.9}\square_{0.1}O_2$, respectively, in which vacancy of the Mn site is expressed by □. Note that possible honeycomb-type charge ordering of $Mn^{III}/Mn^{IV} = 2:1$ is thought to stabilize the *o*-NMO phase. Regarding the unassigned peak of *o*-NMO at $2\theta = 7.8°$, a transmission electron microscope (TEM) image along [001] for *o*-NMO clearly indicates strong subspots of electron diffractions originating from an in-plane superstructure with $6a_{ortho}$*$4b_{ortho}$ units (Figure 1 c), which was not observed previously to the best of our knowledge. By using a larger unit cell, the peak at $2\theta = 7.8°$ can be assigned to an 1/2 1/2 2 index. In Figure 1 f, streaky patterns along [100] of *h*-NMO imply existence of stacking faults resulting from the Mn defect. Furthermore, the possibility of Mn vacancy ordering along ⟨310⟩ for *h*-NMO (Figure 1 e) similar to that of $Na_2Mn_3O_7$[13] and a *c*-axial superstructure for *o*-NMO (Figure 1 d) is also confirmed. SXRD, TEM, and electron diffraction results convinced the successful single-phase formation of $Na_{2/3}MnO_2$ polymorphs; mamely, *o*-NMO has a remarkable CJTD without a Mn vacancy, although *h*-NMO has a Mn vacancy without distortion.

Their electrochemical properties of *o*- and *h*-NMO were further investigated in nonaqueous Na cells, and charge/discharge curves are represented in Figure 2. *o*- and *h*-NMO show different first charge capacities of 142 and 94 mAh g^{-1}, corresponding to 0.54 and 0.37 Na extraction, which are

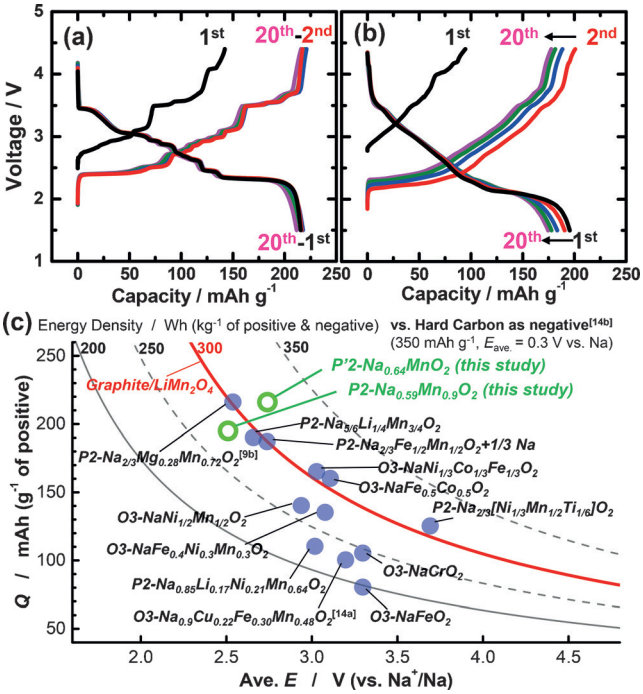

Figure 2. Charge–discharge curves of a) *o*-NMO and b) *h*-NMO between 4.4–1.5 V and c) average voltage versus gravimetric capacity plots for reported positive materials with calculated energy density curves.[3a,9b,14]

consistent with oxidation up to +4 from +3.37 and +3.76 of Mn (Table 1), respectively. *o*-NMO delivers the larger reversible capacity of 216 mAh g^{-1} with average working voltage of about 2.74 V, demonstrating the higher energy density of circa 590 Wh (kg-oxide)$^{-1}$ than 520 Wh (kg-oxide)$^{-1}$ for P2-$Na_xFe_{1/2}Mn_{1/2}O_2$.[2] On the other hand, *h*-NMO has relatively smooth curves, and its energy density is 490 Wh (kg-oxide)$^{-1}$ with initial reversible capacity of 198 mAh g^{-1}. Figure 2 c summarizes the energy density map of sodium-ion cells with reported positive materials and hard-carbon anodes.[3a,9b,14] For a hard carbon//*o*-NMO full cell, the calaculated energy density is more than 300 Wh kg^{-1}. Moreover, *o*-NMO shows excellent cycle stability, and more than

94% of initial discharge capacity is retained after 25 cycles (Supporting Information, Figure S4), despite of the strong distortion and multiple-stepswise profiles indicating phase transitions. dQ/dV plots of *o*-NMO show highly reversible and stable profiles during cycles. For *h*-NMO, however, the capacity degradation is unavoidable unless limiting cut-off voltage (Supporting Information, Figure S4). The irreversible change of reduction peak below 2.2 V is seen in dQ/dV plots of *h*-NMO, suggesting structural change (Supporting Information, Figure S5). Inferior rate property of *h*-NMO to *o*-NMO is evidenced (Supporting Information, Figure S6), probably because the 10% Mn defects induce severe charge disorder in the $Mn_{0.9}O_2$ slab and deterioration of Na^+ duffusivity. Since particle size (ca. 5 μm) and morphology of both samples are identical (Supporting Information, Figure S3), the only explanation for these different electrochemical properites can be laid on crystal structure including CJTD, long-range ordering, and different Mn stoichiometry of these polymorphs.

Structural evolution during the initial galvanostatic cycle was further studied with operando XRD, as shown in Figure 3. The P′2 phase (denoted as P′2-I in the Figure) of *o*-NMO is maintained in $0.25 < x < 0.80$ in Na_xMnO_2, and changed into OP4 phase in $x < 0.3$ during charge. OP4-phase is also confirmed by ex situ XRD (Supporting Information, Figure S7a).[2,7b] Furthermore, we simulate XRD patterns by introducing stacking faults of randam O/P staking into the OP4-type structure by the DIFFaX program and obtain better agreement with the experimental XRD pattern of the sample charged to 4.4 V (see the detailed results in the Supporting Information, Figure S7). During discharge, the OP4 phase reversiblly transforms to P′2-I and finally to different P′2 phase (P′2-II) in $x > 0.64$. Furthermore, clear stepwise change in position of 022 diffraction is observed in P′2-I phase, and the step intervals are consistent with the charge/discharge curves. Totally, 7 sub-phases, P′2-$l_{(1-7)}$ can be seen in $0.2 < x < 0.6$ as marked with white dashed lines in Figure 3a. Given CJTD effects along the *b*-axis, complicated stepwise behavior of 022 line suggests interaction between Na/vacancy and $Mn^{III/IV}$ charge orderings via CJTD. Such interactive coupling has also been reported in O′3-Na_xMnO_2,[15] and the detailed structural study of *o*-NMO is now under way and will be reported elsewhere.

Meanwhile, *h*-NMO shows moderate phase changes in Figure 3b. P′2-phase (P′2-lll) having distorted lattice, similar to P′2-ll phase of *o*-NMO, appears on the discharge below 2.2 V ($x > 0.67$ in $Na_xMn_{0.9}O_2$) owing to increase in Mn^{III} ions, as is also evidenced by ex situ XRD in the Supporting Information, Figure S7b. The limited x range of distorted P′2 phase ($x > 0.67$) compared to *o*-NMO ($x > 0.22$) implies depression of co-operative lattice distortion by the Mn defects. The change of lattice parameters, degree of in-plane distortion, and lattice volume during the first cycle is summarized in the Supporting Information, Figure S8. The volume change is at most 9% for *o*-NMO and only 2.5% for *h*-NMO. Furthermore, the degree of in-plane distortion, δ, drastically changes from zero to 10% during the first discharge for *o*-NMO. Despite of those severe changes, *o*-NMO demonstrates the superior cycle stability and highly

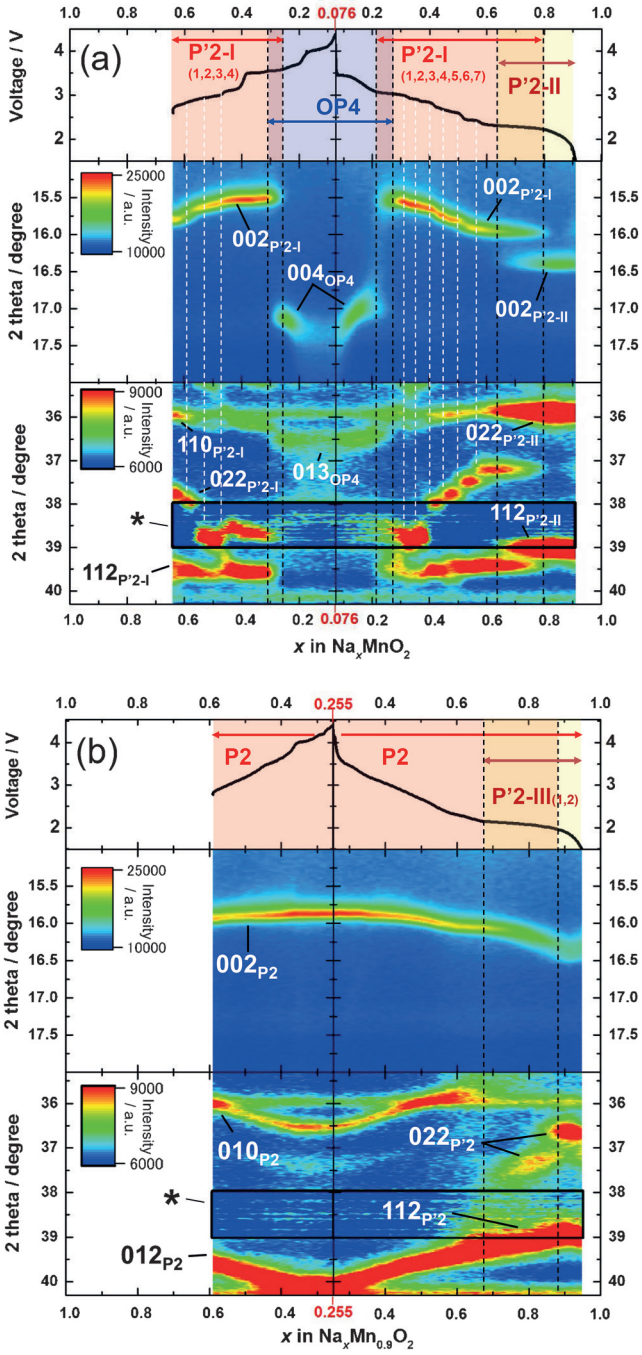

Figure 3. The initial charge–discharge cuves and phase evolution (top) and contour maps of operando XRD patterns for a) *o*-NMO and b) *h*-NMO. The diffraction intensity in the region marked ⋆ is treated by substracting the background diffraction of the beryllium window.

reversible phase transitions. On the other hand, capacity degradation of *h*-NMO is mainly observed below 2.2 V, where the P2 and P′2-lll bi-phasic region appears, as indictated in cyclability and dQ/dV plots (Figures 2b; Supporting Information, Figure S5). Thus, localized distortion with Mn defect and Jahn–Teller Mn^{III} ions possibly induce irreversible structural change, leading to the faster capacity decay. From these results, the highly reversible phase transitions and

excellent electrochemical performance are believed to be due to positive effect of the co-operative distortion of *o*-NMO.

In summary, the precise single-phase preparation of P2 and P′2-$Na_{2/3}MnO_2$ is found and it enables to demonstrate superior battery performance of *o*-NMO for a highly energetic Na-ion battery. The Mn defect is a key factor leading to unfavorable effects on electrochemical properties, and CJTD does not deteriorate reversible Na intercalation for *o*-NMO. We will further study and report their physical properties correlated with manganese and sodium stoichiometry and Jahn–Teller distortion.

Acknowledgements

The authors thank Dr. Ichihashi and Prof. Idemoto, TUS, for TEM measurements. This study was in part granted by JSPS KAKENHI Grant Number JP 16H04225. The synchrotron radiation experiments were performed at the BL02B2 of SPring-8 with the approval of the JASRI (Proposal No. 2014B1820 and 2015A1881).

Keywords: Jahn–Teller distortion · layered compounds · polymorphism · positive electrode materials · sodium-ion batteries

How to cite: *Angew. Chem. Int. Ed.* **2016**, *55*, 12760–12763
Angew. Chem. **2016**, *128*, 12952–12955

[1] B. Dunn, H. Kamath, J. M. Tarascon, *Science* **2011**, *334*, 928–935.
[2] N. Yabuuchi, M. Kajiyama, J. Iwatate, H. Nishikawa, S. Hitomi, R. Okuyama, R. Usui, Y. Yamada, S. Komaba, *Nat. Mater.* **2012**, *11*, 512–517.
[3] a) N. Yabuuchi, K. Kubota, M. Dahbi, S. Komaba, *Chem. Rev.* **2014**, *114*, 11636–11682; b) R. J. Clément, P. G. Bruce, C. P. Grey, *J. Electrochem. Soc.* **2015**, *162*, A2589–A2604.
[4] J.-P. Parant, R. Olazcuaga, M. Devalette, C. Fouassier, P. Hagenmuller, *J. Solid State Chem.* **1971**, *3*, 1–11.
[5] C. Delmas, C. Fouassier, P. Hagenmuller, *Physica B* **1980**, *99*, 81–85.
[6] A. Mendiboure, C. Delmas, P. Hagenmuller, *J. Solid State Chem.* **1985**, *57*, 323–331.
[7] a) A. Caballero, L. Hernán, J. Morales, L. Sánchez, J. Santos Peña, M. A. G. Aranda, *J. Mater. Chem.* **2002**, *12*, 1142–1147; b) J. Billaud, G. Singh, A. R. Armstrong, E. Gonzalo, V. Roddatis, M. Armand, T. Rojo, P. G. Bruce, *Energy Environ. Sci.* **2014**, *7*, 1387.
[8] a) Q. Huang, M. L. Foo, R. A. Pascal, J. W. Lynn, B. H. Toby, T. He, H. W. Zandbergen, R. J. Cava, *Phys. Rev. B* **2004**, *70*, 184110; b) C. Didier, M. Guignard, J. Darriet, C. Delmas, *Inorg. Chem.* **2012**, *51*, 11007–11016.
[9] a) N. Yabuuchi, R. Hara, M. Kajiyama, K. Kubota, T. Ishigaki, A. Hoshikawa, S. Komaba, *Adv. Energy Mater.* **2014**, *4*, 1301453; b) N. Yabuuchi, R. Hara, K. Kubota, J. M. Paulsen, S. Kumakura, S. Komaba, *J. Mater. Chem. A* **2014**, *2*, 16851–16855; c) D. Buchholz, C. Vaalma, L. G. Chagas, S. Passerini, *J. Power Sources* **2015**, *282*, 581–585.
[10] a) J. M. Paulsen, J. R. Dahn, *Solid State Ionics* **1999**, *126*, 3–24; b) R. Stoyanova, D. Carlier, M. Sendova-Vassileva, M. Yoncheva, E. Zhecheva, D. Nihtianova, C. Delmas, *J. Solid State Chem.* **2010**, *183*, 1372–1379.
[11] a) L. Bordet-Le Guenne, P. Deniard, P. Biensan, C. Siret, R. Brec, *J. Mater. Chem.* **2000**, *10*, 2201–2206; b) C. Fouassier, C. Delmas, P. Hagenmuller, *Mater. Res. Bull.* **1975**, *10*, 443–449.
[12] F. Izumi, K. Momma, *Solid State Phenom.* **2007**, *130*, 15–20.
[13] a) F. M. Chang, M. Jansen, *Z. Anorg. Allg. Chem.* **1985**, 531; b) E. A. Raekelboom, A. L. Hector, J. Owen, G. Vitins, M. T. Weller, *Chem. Mater.* **2001**, *13*, 4618–4623.
[14] a) L. Mu, S. Xu, Y. Li, Y. S. Hu, H. Li, L. Chen, X. Huang, *Adv. Mater.* **2015**, *27*, 6928–6933; b) H. Yamamoto, K. Kubota, M. Fukunishi, A. Watanabe, T. Kim, S. Komaba, 83rd meeting of Electrochem. Soc. Japan, **2016**, Osaka.
[15] X. Li, X. Ma, D. Su, L. Liu, R. Chisnell, S. P. Ong, H. Chen, A. Toumar, J. C. Idrobo, Y. Lei, J. Bai, F. Wang, J. W. Lynn, Y. S. Lee, G. Ceder, *Nat. Mater.* **2014**, *13*, 586–592.

Received: July 2, 2016
Published online: September 15, 2016

